

## ARTICLE TYPE

## A correlation for average droplet diameter in rotating packed beds

Shahab Golshan<sup>1</sup> | Alireza Shams<sup>2</sup> | Roshanak Rabiee<sup>2</sup> | Rouzbeh Jafari<sup>2</sup> | Jamal Chaouki<sup>\*2</sup> | Bruno Blais<sup>\*\*1</sup>

<sup>1</sup>Chemical Engineering, Research Unit for Industrial Flows Processes (URPEI), Department of Chemical Engineering, Polytechnique Montréal, C.P. 6079, Succ. "CV", Montréal, H3C 3A7 Québec, Canada

<sup>2</sup>Chemical Engineering, Polytechnique Montréal, Process Engineering Advanced Research Lab (PEARL), C.P. 6079, Succ. "CV", Montréal, H3C 3A7 Québec, Canada

## Correspondence

Corresponding authors:

\*J. Chaouki, Polytechnique Montreal.

Email: jamal.chaouki@polymtl.ca

\*\*B. Blais, Polytechnique Montreal.

Email: bruno.blais@polymtl.ca

## Abstract

Rotating packed bed (RPB) is a novel process intensification technology that increases mass transfer rate using a strong centrifugal acceleration. Inside an RPB, the inlet jet of the liquid absorbent is broken into tiny droplets. It is reported that RPBs provide 11 times larger mass transfer area compared to equal-sized packed beds and 2-3 orders of magnitude higher mass transfer compared to equal-sized stirred tanks. The novelty of the technology and lack of research, however, undermines the adoption of RPBs where a low mass transfer rate is the main bottleneck. In this work, we study the effect of bed size on the average droplet diameter in rotating packed beds and investigate scale-up criteria to preserve the average droplet diameter at a large scale. Furthermore, we develop a correlation for the average droplet diameter using the experimental data and simulation results obtained using a Volume of Fluid (VOF) method. This correlation is obtained from dimensional analysis. The effects of rotating speed, absorbent flow rate, wire mesh packing diameter, bed diameter, absorbent viscosity, density, and surface tension are included in the dataset. Among these parameters, rotating speed, centrifugal force, and surface tension have the highest correlation coefficients ( $R^2 = 0.88, 0.83$ , and  $0.42$ , respectively) with the average droplet diameter.

## KEYWORDS:

Rotating Packed Bed, Computational Fluid Dynamics (CFD), Carbon Capture, Volume of Fluid (VOF), Process Intensification

## 1 | INTRODUCTION

According to the Intergovernmental Panel on Climate Change (IPCC), the average global temperature will increase by  $1.1 - 2^\circ\text{C}$  before 2050, due to emissions of greenhouse gasses<sup>[1, 2]</sup>. Carbon dioxide ( $\text{CO}_2$ ) is the main contributor ( $\approx 60\%$ ) to global warming<sup>[3]</sup>. IPCC states that the global  $\text{CO}_2$  emissions should be decreased by 50% before 2050<sup>[2]</sup>. This is against the trends of  $\text{CO}_2$  emissions and global average temperature during the recent years. Consequently, researchers are looking

for efficient and operational carbon-capture technologies. Mass transfer rate is the most significant parameter on the carbon-capture efficiency<sup>[4]</sup>. Rotating packed bed (RPB) is a novel operating unit that accelerates mass transfer using strong centrifugal acceleration<sup>[5, 6]</sup>.

RPB is a gas-liquid contactor which can be used for  $\text{CO}_2$  capture and acid gas removal from a gas stream using an amine-based liquid<sup>[7, 8]</sup>. RPB consists of a hollow cylindrical vessel filled with a packing material (mainly wire mesh or Nickel foam)<sup>[8-12]</sup>. The packing rotates at a high speed ( $\approx 250-1500$  rpm) and breaks the inlet liquid stream into filaments and droplets<sup>[9, 13]</sup>. This breaking

process greatly increases the mass transfer area in RPBs ( $\approx 11$  times larger than a packed bed with equal size), leading to higher efficiency compared to conventional packed beds<sup>[5]</sup>. This higher efficiency enables the use of a smaller volume of rotating packed bed ( $\approx 9\%$  of the fixed bed volume) while obtaining an equal mass transfer<sup>[5]</sup>. Compared to stirred tank reactors, RPBs obtain 2-3 order of magnitude higher mass transfer<sup>[14]</sup>.

Despite the potential of RPBs, the technology is still developing and several design and scale-up uncertainties limits industrial deployment of RPB.<sup>[15, 16]</sup> Understanding and being able to predict the hydrodynamics of the multi-phase flow within RPBs is one of these challenges. This is in part caused by the small size ( $O(100\mu\text{m})$ ) and large number of droplets inside the bed<sup>[13, 15, 17]</sup>. The number and size of droplets dictate the mass transfer area in the bed. Researchers have used experimental and simulation methods to measure the droplet size in RPBs<sup>[13, 15, 18–20]</sup>. Sang et al.<sup>[18, 19]</sup> studied the effects of rotating speed, liquid viscosity, and surface tension on the average droplet diameter using a high-speed camera. They observed that with increasing rotating speed, and decreasing surface tension, average droplet size decreases. These observations were verified by Liu et al.<sup>[13, 17]</sup> who measured the average droplet diameter using a high-speed camera. They also observed that liquid flow rate does not have any effect on the average droplet diameter. Ghadyanlou et al.<sup>[21]</sup> reviewed the correlations for the estimation of liquid element thickness in rotating packed beds. It is also possible to predict the droplet size using Computational Fluid Dynamics (CFD) simulations<sup>[15]</sup>. Researchers in this field mainly use Volume of Fluid (VOF) method to study the hydrodynamics of RPBs in micro-scale<sup>[11, 15, 22, 23]</sup>.

The amount of research on the average droplet size and mass transfer area in RPBs is very limited<sup>[13, 15, 17]</sup>. The main challenge in measuring the droplet size in CFD simulations is the high mesh resolution required to get grid-converged droplet size distribution<sup>[15, 22]</sup>. This issue limits the size of the RPBs that can be simulated using VOF strategies. In this research, we simulate thirty six RPBs with different rotating speeds, surface tensions, absorbent inlet velocities and bed sizes to study the effects of mentioned parameters on the average droplet diameter. To the best of authors knowledge, this research is the first study the of the effect of bed size on the average droplet diameter. We conduct a dimensional analysis on the effective parameters, and use the simulation results and the experimental data of Liu et al.<sup>[13, 17]</sup> to propose a correlation to estimate the average droplet diameter in RPBs.

## 2 | MODELS AND METHODS

We used a VOF model to simulate the RPBs. The inter-FOAM solver in OpenFOAM<sup>[24]</sup> was used for the simulations. In our previous work<sup>[15]</sup>, we observed that the droplet size distributions obtained from two-dimensional and three-dimensional simulations of RPBs are almost identical. As a result, we use two-dimensional VOF simulations in the current research. This strategy was also used by other researchers<sup>[10, 25, 26]</sup> to study liquid holdup and droplet size inside RPBs.

### 2.1 | Volume of fluid model

The VOF model was proposed by Hirt and Nichols<sup>[27]</sup>. In it, continuity and conservation of momentum are described using the Navier-Stokes equations:

$$\nabla \cdot \mathbf{u} = 0 \quad (1)$$

$$\frac{\partial(\rho \mathbf{u})}{\partial t} + \nabla \cdot (\rho \mathbf{u} \mathbf{u}) = -\nabla p + \nabla \cdot \bar{\bar{\tau}} + \rho \mathbf{g} + \mathbf{f}_\sigma \quad (2)$$

where  $\mathbf{u}$  is the fluid velocity,  $t$  is time,  $\rho$  denotes the density of the fluid,  $p$  is pressure,  $\bar{\bar{\tau}}$  is the deviatoric stress tensor,  $\mathbf{g}$  shows the gravitational acceleration, and  $\mathbf{f}_\sigma$  denotes the continuum surface force (surface tension force converted into a volumetric force). The following equation defines  $\mathbf{f}_\sigma$ :

$$\mathbf{f}_\sigma = \sigma k \nabla \alpha_i \quad (3)$$

where

$$k = -\nabla \cdot \left( \frac{\nabla \alpha_i}{|\nabla \alpha_i|} \right) \quad (4)$$

and  $\alpha_i$  is the volume fraction of phase  $i$  (liquid or gas),  $\rho$  and  $\mu$  are density and viscosity of the grid cell, which are defined as:

$$\rho = \alpha_l \rho_l + \alpha_g \rho_g \quad (5)$$

$$\mu = \alpha_l \mu_l + \alpha_g \mu_g \quad (6)$$

The following equation is solved in order to track the interphase between gas and liquid:

$$\frac{\partial \alpha_l}{\partial t} + \nabla \cdot (\alpha_l \mathbf{u}) = 0 \quad (7)$$

A sliding mesh model using Arbitrary Mesh Interface (AMI) rotates the packing zone of the mesh. AMI performs this mesh motion and ensures that the fluxes are conserved at the interface of the rotating and static regions. For this purpose, we need separate meshes for the rotating and static regions of the RPB. `cyclicAMI` boundary condition couples the static and rotating regions at the patch boundaries. More information on the theory and implementation of the AMI can be found elsewhere<sup>[28]</sup>.

TABLE 1 Simulation and experimental<sup>[13]</sup> data on average droplet diameter at different rotating speeds, absorbent flow rates, bed sizes, packing wire diameters and various absorbents (with various viscosities, surface tension and densities).

No.	Ref.	$\omega(\text{rad s}^{-1})$	$u(\text{m s}^{-1})$	$\mu(\text{mPa s})$	$\sigma(\text{N m}^{-1})$	$d_p(\text{mm})$	$\rho(\text{kg m}^{-3})$	$n_p$	$\bar{D}_p(\text{m})$	$\bar{d}_d(\text{mm})$
1	VOF	26.18	1.5	1	0.07	0.5	1000	21	0.066	0.7209
2	VOF	26.18	2	1	0.07	0.5	1000	21	0.066	0.7786
3	VOF	26.18	2.87	1	0.07	0.5	1000	21	0.066	0.7317
4	VOF	52.36	1.5	1	0.07	0.5	1000	21	0.066	0.5736
5	VOF	52.36	2	1	0.07	0.5	1000	21	0.066	0.5412
6	VOF	52.36	2.87	1	0.07	0.5	1000	21	0.066	0.5554
7	VOF	104.72	1.5	1	0.07	0.5	1000	21	0.066	0.3247
8	VOF	104.72	2	1	0.07	0.5	1000	21	0.066	0.3281
9	VOF	104.72	2.87	1	0.07	0.5	1000	21	0.066	0.3315
10	VOF	157.08	1.5	1	0.07	0.5	1000	21	0.066	0.2816
11	VOF	157.08	2	1	0.07	0.5	1000	21	0.066	0.2803
12	VOF	157.08	2.87	1	0.07	0.5	1000	21	0.066	0.2824
13	VOF	52.36	1.5	1	0.01	0.5	1000	21	0.066	0.2805
14	VOF	52.36	1.5	1	0.15	0.5	1000	21	0.066	0.7062
15	VOF	42.73	4.305	1	0.07	0.5	1000	32	0.099	0.4917
16	VOF	85.45	4.305	1	0.07	0.5	1000	32	0.099	0.3707
17	VOF	128.08	4.305	1	0.07	0.5	1000	32	0.099	0.2815
18	VOF	21.36	2.25	1	0.07	0.5	1000	32	0.099	0.7127
19	VOF	42.73	2.25	1	0.07	0.5	1000	32	0.099	0.5574
20	VOF	85.45	2.25	1	0.07	0.5	1000	32	0.099	0.4148
21	VOF	128.08	2.25	1	0.07	0.5	1000	32	0.099	0.3094
22	VOF	42.73	3	1	0.07	0.5	1000	32	0.099	0.4979
23	VOF	85.45	3	1	0.07	0.5	1000	32	0.099	0.3832
24	VOF	128.08	3	1	0.07	0.5	1000	32	0.099	0.3065
25	VOF	18.54	5.74	1	0.07	0.5	1000	43	0.132	0.7785
26	VOF	37.07	5.74	1	0.07	0.5	1000	43	0.132	0.5517
27	VOF	74.03	5.74	1	0.07	0.5	1000	43	0.132	0.3664
28	VOF	111.11	5.74	1	0.07	0.5	1000	43	0.132	0.3045
29	VOF	18.54	4	1	0.07	0.5	1000	43	0.132	0.7486
30	VOF	37.07	4	1	0.07	0.5	1000	43	0.132	0.5729
31	VOF	74.03	4	1	0.07	0.5	1000	43	0.132	0.37
32	VOF	111.11	4	1	0.07	0.5	1000	43	0.132	0.3243
33	VOF	18.54	3	1	0.07	0.5	1000	43	0.132	0.7187
34	VOF	37.07	3	1	0.07	0.5	1000	43	0.132	0.5517
35	VOF	74.03	3	1	0.07	0.5	1000	43	0.132	0.3664
36	VOF	111.11	3	1	0.07	0.5	1000	43	0.132	0.3045
37	[13]	41.887	3.095	1.004	0.0727	0.45	999	12	0.172	0.6982
38	[13]	62.832	3.095	1.004	0.0727	0.45	999	12	0.172	0.5563
39	[13]	83.776	3.095	1.004	0.0727	0.45	999	12	0.172	0.3961
40	[13]	104.72	3.095	1.004	0.0727	0.45	999	12	0.172	0.3286
41	[13]	125.66	3.095	1.004	0.0727	0.45	999	12	0.172	0.3103
42	[13]	41.887	3.095	1.004	0.0727	0.18	999	12	0.172	0.6719
43	[13]	62.832	3.095	1.004	0.0727	0.18	999	12	0.172	0.5014
44	[13]	83.776	3.095	1.004	0.0727	0.18	999	12	0.172	0.3812
45	[13]	104.72	3.095	1.004	0.0727	0.18	999	12	0.172	0.3263

Continued on next page

TABLE 1 – Continued from previous page

No.	Ref.	$\omega(\text{rad s}^{-1})$	$u(\text{m s}^{-1})$	$\mu(\text{mPa s})$	$\sigma(\text{N m}^{-1})$	$d_p(\text{mm})$	$\rho(\text{kg m}^{-3})$	$n_p$	$\bar{D}_p(\text{m})$	$\bar{d}_d(\text{mm})$
46	[13]	125.66	3.095	1.004	0.0727	0.18	999	12	0.172	0.3046
47	[13]	83.776	2.21	1.004	0.0727	0.45	999	12	0.172	0.3430
48	[13]	83.776	2.653	1.004	0.0727	0.45	999	12	0.172	0.3364
49	[13]	83.776	3.538	1.004	0.0727	0.45	999	12	0.172	0.3397
50	[13]	83.776	3.98	1.004	0.0727	0.45	999	12	0.172	0.3331
51	[13]	62.832	2.21	1.004	0.0727	0.45	999	12	0.172	0.5331
52	[13]	62.832	2.653	1.004	0.0727	0.45	999	12	0.172	0.5397
53	[13]	62.832	3.538	1.004	0.0727	0.45	999	12	0.172	0.5496
54	[13]	62.832	3.98	1.004	0.0727	0.45	999	12	0.172	0.5132
55	[13]	41.887	2.21	1.004	0.0727	0.45	999	12	0.172	0.7066
56	[13]	41.887	2.653	1.004	0.0727	0.45	999	12	0.172	0.7132
57	[13]	41.887	3.538	1.004	0.0727	0.45	999	12	0.172	0.7198
58	[13]	41.887	3.98	1.004	0.0727	0.45	999	12	0.172	0.7281
59	[13]	41.887	3.095	1.004	0.043	0.45	999	12	0.172	0.4927
60	[13]	62.832	3.095	1.004	0.043	0.45	999	12	0.172	0.3442
61	[13]	83.776	3.095	1.004	0.043	0.45	999	12	0.172	0.3267
62	[13]	104.72	3.095	1.004	0.043	0.45	999	12	0.172	0.2670
63	[13]	125.66	3.095	1.004	0.043	0.45	999	12	0.172	0.2655
64	[13]	83.776	3.095	2.517	0.0709	0.45	1072	12	0.172	0.3970
65	[13]	83.776	3.095	3.783	0.07	0.45	1099	12	0.172	0.3905
66	[13]	83.776	3.095	6.053	0.0689	0.45	1126	12	0.172	0.3857
67	[13]	83.776	3.095	10.944	0.0679	0.45	1153	12	0.172	0.3776
68	[13]	83.776	3.095	22.951	0.067	0.45	1181	12	0.172	0.3501
69	[13]	41.887	3.095	2.517	0.0709	0.45	1072	12	0.172	0.7381
70	[13]	41.887	3.095	3.783	0.07	0.45	1099	12	0.172	0.7349
71	[13]	41.887	3.095	6.053	0.0689	0.45	1126	12	0.172	0.7316
72	[13]	41.887	3.095	10.944	0.0679	0.45	1153	12	0.172	0.7268
73	[13]	41.887	3.095	22.951	0.067	0.45	1181	12	0.172	0.7203
74	[18]	73.3	1.965	1.12	0.0731	0.22	999	3	0.2305	0.6402
75	[18]	94.25	1.965	1.12	0.0731	0.22	999	3	0.2305	0.5614
76	[18]	115.192	1.965	1.12	0.0731	0.22	999	3	0.2305	0.5182
77	[18]	52.36	1.965	1.12	0.0387	0.22	999	3	0.2305	0.7174
78	[18]	73.304	1.965	1.12	0.0387	0.22	999	3	0.2305	0.6065
79	[18]	94.248	1.965	1.12	0.0387	0.22	999	3	0.2305	0.5152
80	[18]	115.192	1.965	1.12	0.0387	0.22	999	3	0.2305	0.4848
81	[18]	52.36	1.965	1.12	0.0731	0.22	999	4	0.2505	0.7260
82	[18]	52.36	1.965	1.12	0.0731	0.22	999	5	0.2705	0.7272
83	[18]	52.36	1.965	1.12	0.0731	0.22	999	6	0.2905	0.6046
84	[18]	52.36	1.965	1.12	0.0731	0.22	999	7	0.3105	0.5745
85	[18]	94.248	1.965	1.12	0.0731	0.22	999	2	0.2105	0.5518
86	[18]	94.248	1.965	1.12	0.0731	0.22	999	3	0.2305	0.5411
87	[18]	94.248	1.965	1.12	0.0731	0.22	999	4	0.2505	0.4991
88	[18]	94.248	1.965	1.12	0.0731	0.22	999	5	0.2705	0.4989
89	[18]	94.248	1.965	1.12	0.0731	0.22	999	6	0.2905	0.4702
90	[18]	94.248	1.965	1.12	0.0731	0.22	999	7	0.3105	0.4327



## 2.2 | Post-processing

We use a post-processing code written in Matlab to obtain the droplet size distribution and average droplet size inside the RPBs. This code uses image-processing to detect distinct droplets, and calculates the equivalent droplet diameter ( $d_d$ ) using the following equation:

$$d_d = \sqrt{\frac{4A_d}{\pi}} \quad (8)$$

where  $A_d$  denotes the droplet area. We used this approach in our previous study<sup>[15]</sup>. We performed a sensitivity analysis on the image resolution (number of pixels), and obtained the minimum pixel number that does not have a significant effect on the calculated droplet size distributions. Furthermore, we performed grid dependence analyses on the RPBs with different diameters and rotating speeds. According to these analyses, maximum mesh sizes of 100  $\mu\text{m}$  and 42  $\mu\text{m}$  were chosen for RPBs operating at  $\omega \leq 500$  rpm and  $500 \text{ rpm} < \omega \leq 1500$  rpm, respectively.

## 2.3 | Configurations used

Thirty six VOF simulations and fifty four experimental data<sup>[13, 18]</sup> at different rotating speeds, absorbent flow rates, bed sizes, packing wire diameters and various absorbents (with various viscosities, surface tension and densities) are used to obtain the correlation. Table 1 reports these simulation and experimental data. The data are also available in a github repository: [https://github.com/shahabgol/RPB\\_data.git](https://github.com/shahabgol/RPB_data.git)

## 2.4 | RPB geometry

Figure 1 shows the geometries of the simulated RPBs in this work. As mentioned in Table 1, we use three different bed sizes,  $D_b = 0.09 \text{ m}$ ,  $0.135 \text{ m}$ , and  $0.18 \text{ m}$ , ( $\bar{D}_p = 0.066 \text{ m}$ ,  $0.099 \text{ m}$ , and  $0.132 \text{ m}$ , respectively) in the simulations. The wire mesh packing elements have a maximum azimuthal distance of 3.5 mm and maximum radial distance of 1 mm, as illustrated in Figure 2. We choose this wire mesh pattern according to the packing design used by Xie et al.<sup>[25]</sup> and Yang et al.<sup>[9]</sup>. Based on the scale-up criteria proposed by Liu et al.<sup>[13, 17]</sup>, we keep the values of  $D_b\omega^2$  and  $Q_l/V_b$  constant in our simulation table, where  $Q_l$  is the volumetric flow rate of the absorbent. Furthermore, the ratio of packing length to bed diameter is constant in the simulations. The packing geometry and design do not change when increasing the bed size (only the number of wire mesh layers increase to maintain the ratio of the packing length to the bed diameter)

according to the recommendation of Liu et al.<sup>[13]</sup>. Table 1 reports the physical properties of the absorbent used in the simulations.

## 3 | RESULTS AND DISCUSSION

### 3.1 | Mesh independence and validation

We have performed mesh independence analysis and validation of the model in our previous work<sup>[15]</sup> on the same RPB. Figure 3 shows an example of the performed grid independence analyses at  $u = 1.5 \text{ m s}^{-1}$ ,  $\omega = 157.08 \text{ rad s}^{-1}$  and  $D_b = 0.09 \text{ m}$ . Droplet area distribution and droplet number do not change significantly by decreasing the mesh size from 50  $\mu\text{m}$  to 40  $\mu\text{m}$ . We perform a similar grid independence analysis for each simulation in Table 1. We also observed that the two-dimensional simulations are capable of obtaining the correct droplet size distributions by comparing to the three-dimensional simulations, and verified that the mesh sizes are chosen adequately fine to capture the significant turbulent structures in the studied RPBs<sup>[15]</sup>. Figure 4 shows a comparison between the droplet area distributions obtained from two-dimensional and three-dimensional simulations at  $u = 1.5 \text{ m s}^{-1}$ ,  $\omega = 52.36 \text{ rad s}^{-1}$ ,  $l_m = 100 \mu\text{m}$  and  $D_b = 0.09 \text{ m}$ . This analysis verifies that the droplet sizes calculated from two-dimensional and three-dimensional simulations are identical. Comparison of the average droplet sizes from this work and experimental results of<sup>[13, 18]</sup> in the following sections further verify the validation of our model.

### 3.2 | Average droplet diameter

We calculate the coefficients of determination between average droplet diameters and rotating speed, absorbent velocity, viscosity, density, surface tension, packing diameter, and bed size using the data in Table 1. The coefficient of determination is defined as:

$$R^2 = \left( \frac{\text{COV}(x, y)}{S_x S_y} \right)^2 \quad (9)$$

where  $\text{COV}(x, y)$  is the covariance of variables  $x$  and  $y$  and  $S$  is the standard deviation. Table 2 reports these coefficients of determination. The reported coefficients determine the significant parameters on the average droplet diameter. The rotating speed ( $\omega$ ) is the parameter which has the most important impact on the average droplet diameter with a determination coefficient of  $R^2 = 0.88$ . The rotating speed may be related to both the shear rate within the RPB and to the centrifugal force. Hence,

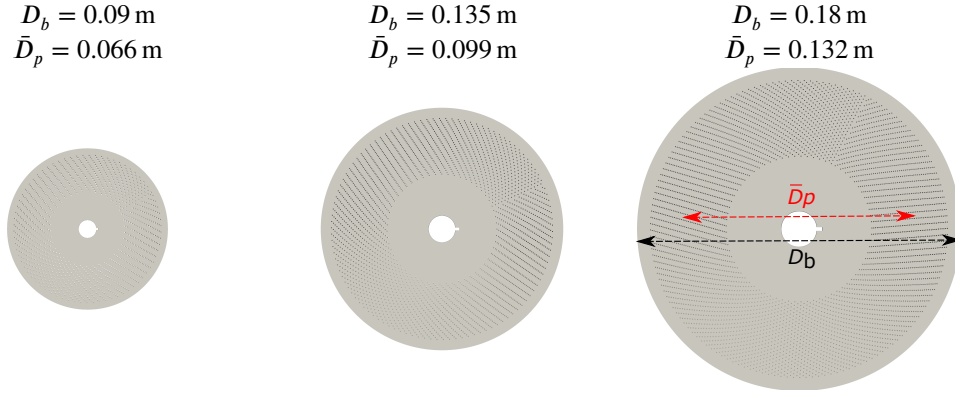


FIGURE 1 Geometries of the three bed sizes used in the VOF simulations.

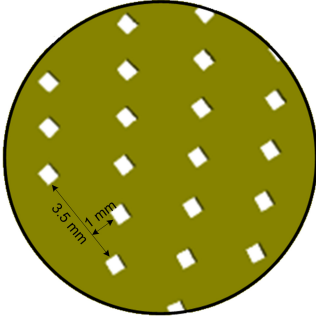


FIGURE 2 Wire mesh packing configuration used in this research. This packing configuration is chosen according to the works of [9, 15, 25].

it's strong correlation with the droplet size if expected. Next to the rotating speed, the centrifugal force  $\rho R_p \omega^2$  is the second-most important parameter. Surface tension ( $\sigma$ ) also plays an important role, with a determination coefficient of  $R^2 = 0.423$ . Other parameters have smaller effects on the average droplet size.

We propose a correlation obtained from dimensional analysis to estimate the average droplet diameter in RPBs. For this purpose, we perform a dimensional analysis on the effective parameters reported in Table 2 using Buckingham  $\pi$  theorem. One of the resulting dimensionless numbers is:

$$\Pi_1 = \frac{1}{n_p} \frac{1}{Bo} = \frac{\sigma}{n_p \rho \bar{D}_p \omega^2 d_d^2} = \frac{\text{cohesion force}}{\text{centrifugal force}} \quad (10)$$

which is the ratio of cohesion force to the centrifugal force.  $n_p$  and  $\bar{D}_p$  denote the number of packing layers and average diameter of the packing zone, respectively. Average diameter of the packing zone is the average of the inner and outer packing zone diameters (see Figure2). In the

Parameter	$R^2$
$\omega$	0.880
$u$	0.001
$\mu$	0.189
$\sigma$	0.423
$d_p$	0.048
$\rho$	0.164
$\bar{D}_p$	0.327
$\bar{R}_p \omega^2$	0.827

TABLE 2 Coefficients of determination between average droplet diameter ( $\bar{d}_d$ ) and rotating speed ( $\omega$ ), absorbent inlet velocity ( $u$ ), viscosity ( $\mu$ ), density ( $\rho$ ), surface tension ( $\sigma$ ), packing diameter ( $d_p$ ), average diameter of the packing zone ( $\bar{D}_p$ ) and  $R_p \omega^2$ .

field of centrifugal microfluidics, the Bond number (Bo) is defined as the ratio of the centrifugal force to the cohesion (surface tension) force [29]:

$$Bo = \frac{\rho D \omega^2 d_d^2}{\sigma} \quad (11)$$

We should mention that although other dimensionless numbers including  $Re = \rho u d_d / \mu$  and  $We = \rho D_b^2 \omega^2 d_d / \sigma$  are also among the results of the dimensional analysis, these dimensionless groups are unable to predict the average droplet diameter accurately. The reason is that these dimensionless groups do not represent the ratio of the dominant forces in rotating packed beds. Droplet diameter can be obtained from  $\Pi_1$  dimensionless number:

$$\bar{d}_d = f \left( \sqrt{\frac{\sigma}{n_p \rho \bar{D}_p \omega^2}} \right) \quad (12)$$

When the RPB reaches steady state condition, the ratio of cohesion force to centrifugal force ( $\Pi_1$ ) reaches an

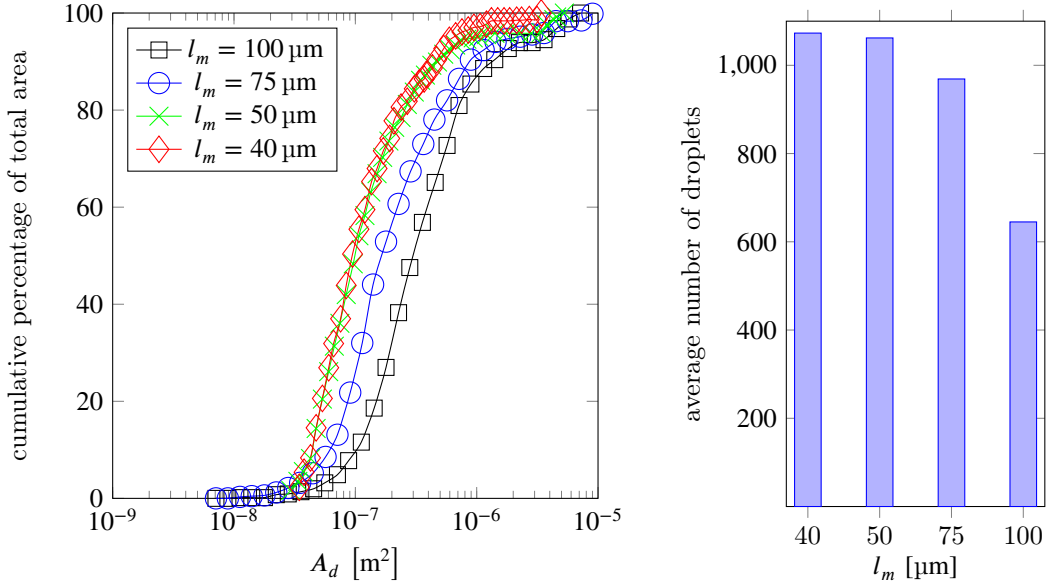


FIGURE 3 Grid independence analysis for RPB operating at  $u = 1.5 \text{ m s}^{-1}$ ,  $\omega = 157.08 \text{ rad s}^{-1}$  and  $\bar{D}_p = 0.066 \text{ m}$ .

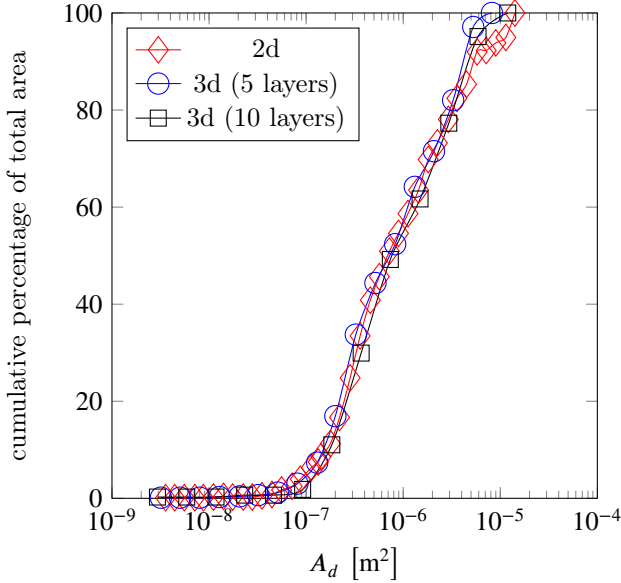


FIGURE 4 Droplet size distributions obtained from the two-dimensional and three-dimensional simulations at  $u = 1.5 \text{ m s}^{-1}$ ,  $\omega = 52.36 \text{ rad s}^{-1}$ ,  $l_m = 100 \mu\text{m}$  and  $D_b = 0.09 \text{ m}$ .

equilibrium:

$$\Pi_1 = C^* \quad (13)$$

where  $C^*$  is a function of the RPB geometry. We obtain the average droplet diameter at the steady state using the

following equation.

$$\bar{d}_d = C^* \sqrt{\frac{\sigma}{n_p \rho \bar{D}_p \omega^2}} \quad (14)$$

We plot average droplet diameters versus  $\sqrt{\frac{\sigma}{n_p \rho \bar{D}_p \omega^2}}$  (we refer to this group as  $\gamma$  for the sake of convenience) in Figure 5. Figure 5 shows two different zones:

- zone I, where  $\gamma < 0.14 \text{ mm}$ . In this zone, the results show a linear increasing trend ( $C^* = 5.185$ ) in the average droplet diameters as a function of  $\gamma$ . Larger centrifugal force breaks the liquid jet into smaller droplets and the droplet diameter decreases with decreasing  $\gamma$ .
- zone II, where  $\gamma \geq 0.14 \text{ mm}$ . In zone II, the absorbent jet breaks into relatively large bulks of liquid via channeling between the wire elements of the packing. Hence, the droplets are formed as liquid bridges between adjacent wire elements and the average droplet diameter is approximately constant. The geometry of the packing governs the average droplet diameter in this zone.

Data from VOF simulations of this work and experiments of Liu et al.<sup>[13]</sup> and Sang et al.<sup>[18]</sup> are used in this figure. Liu et al.<sup>[13]</sup> and Sang et al.<sup>[18]</sup> performed their experiments in a rotating packed bed with different diameter, packing diameter, absorbent properties and absorbent flow rates than the simulations in this research. Nevertheless, their reported droplet diameters fit well to our simulation data when they are plotted against  $\gamma$  in

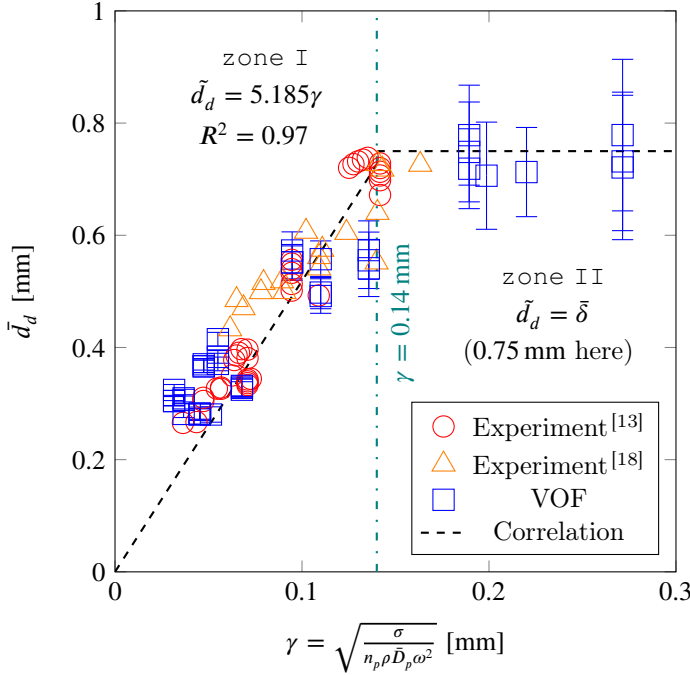


FIGURE 5 Average droplet diameter ( $d_d$ ) as a function of  $\gamma$  for the data in Table 1.

Figure 5. As a result, Figure 5 further proves the conclusion that the rotating speed and surface tension are the dominant parameters on the average droplet diameter. We set the intercept of the trend line in zone I equal to zero, so that with decreasing  $\gamma$  to zero (infinite rotation speed or zero surface tension) the average droplet diameter becomes zero.

Figure 6 shows two sample simulation screenshots of the cases 35 and 33 in Table 1. The top screenshot belong to an RPB operating in zone I with  $\omega = 74.03 \text{ rad s}^{-1}$ , while the bottom screenshot shows a screenshot of an RPB operating in zone II with  $\omega = 18.54 \text{ rad s}^{-1}$ . In zone I, the large centrifugal force breaks the liquid jet into tiny droplets. Golshan et al. discussed the droplet breakup regimes in rotating packed beds<sup>[15]</sup>. zone I in Figure 6 is attributed to shear and catastrophic droplet breakup regimes. On the other hand, in zone II, the liquid jet is broken into separate bulks of liquid in zone II. The droplet breakup mechanism of RPBs operating at zone II are vibrational and bag, and breakup of droplets in this zone is nullified by coalescence<sup>[15]</sup>.

To further evaluate the accuracy of the dimensional analysis, we simulate two RPBs with imaginary absorbents with  $\sigma = 0.01 \text{ N m}^{-1}$  and  $0.15 \text{ N m}^{-1}$  (cases 13 and 14 in Table 1, respectively). The corresponding  $\gamma$

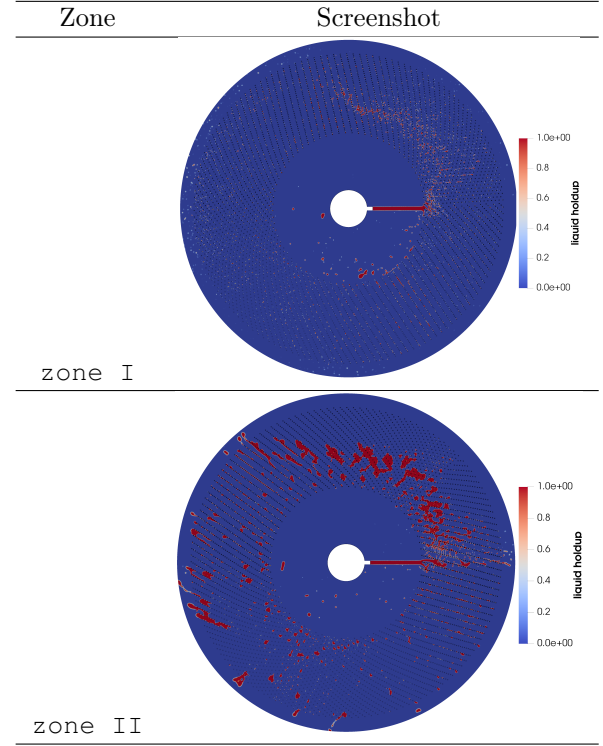


FIGURE 6 Sample screenshots of the RPB simulations operating at top: zone I, and bottom: zone II. The screenshots belong to cases 35 and 33 in Table 1, respectively.

values to these two cases are 0.051 mm and 0.2 mm, respectively. Note that the rotating speed in these cases are  $\omega = 500 \text{ rad s}^{-1}$ . In Figure 7 we compare the screenshots of these two cases with cases 11 and 1, which have similar  $\gamma$  values ( $\gamma = 0.045$  mm and 0.27 mm, respectively). By comparing the screenshots of cases 1 and 14, with  $\gamma > 0.14$  mm (i.e. located in zone II), we observe that the shape and size of droplets are similar. Note that the rotation speed in case 14 ( $\omega = 52.36 \text{ rad s}^{-1}$ ) is twice the rotation speed of case 1 ( $\omega = 26.18 \text{ rad s}^{-1}$ ), while their  $\gamma$  values ( $\gamma \approx 0.23$  mm) are close due to different surface tensions. As a result, the average droplet diameters are also close in these cases. We observe that the droplets in these cases are formed between adjacent wire mesh elements. We conclude that if  $\gamma > 0.14$  mm (i.e. RPB operating in zone II), the rotation of the packing breaks the absorbent jet into liquid bridges between adjacent wire elements. Consequently, the distance between adjacent wire elements of the packing (in this RPB between 0.5 and 1 mm) controls the average droplet size for RPBs operated in zone II ( $\bar{d}_d = 0.75$  mm).

Furthermore, although the rotation speed of case 11 ( $\omega = 157.08 \text{ rad s}^{-1}$ ) is three times larger than the rotation speed of case 13 ( $\omega = 52.36 \text{ rad s}^{-1}$ ), different surface tensions result in similar  $\gamma$  values ( $\gamma \approx 0.047 \text{ mm}$ ). As a result, we observe the same average droplet diameters in these two cases ( $\bar{d}_d = 0.280 \text{ mm}$ ). To sum up, Figure 7 implies two conclusions: the average droplet diameter in zone II is controlled by the distance between adjacent wire packing elements and  $\gamma$  is a trustworthy parameter to predict the mean droplet diameter in RPBs.

Using dimensional analysis, we propose the following correlation, for the estimation of average droplet diameter in RPBs (in the range of geometries investigated in this work).

$$\bar{d}_d = \begin{cases} 5.185\gamma \text{ [mm]}, & \text{if } \gamma < 0.14 \text{ [mm]} \\ \bar{\delta} \text{ [mm]}, & \text{if } \gamma \geq 0.14 \text{ [mm]} \end{cases} \quad (15)$$

where  $\bar{d}_d$  is the estimated droplet diameter using the correlation, and:

$$\gamma = \sqrt{\frac{\sigma}{n_p \rho \bar{D}_p \omega^2}} \quad (16)$$

Figure 8 shows the parity plot for the proposed correlation. Absolute error (AE) is defined as:

$$\text{AE} = \frac{|\bar{d}_d - \bar{d}_d|}{\bar{d}_d} \quad (17)$$

The average absolute error of the proposed correlation is 0.138, which shows its high accuracy. Additionally, this correlation only possesses a single parameter.

### 3.3 | Effects of operating parameters

In our previous research<sup>[15]</sup>, we have studied the effects of rotating speed ( $\omega$ ) and absorbent inlet velocity ( $u$ ) on the average droplet diameter. Increasing the rotating speed decreases the average droplet diameter, while the absorbent inlet velocity does not have a significant effect on the average droplet diameter. Furthermore, the effects of absorbent physical properties were studied<sup>[13, 18]</sup>. Density, and viscosity of the absorbent do not significantly change the average droplet diameter, while increasing surface tension coefficient ( $\sigma$ ), increased average droplet diameter<sup>[13, 18]</sup>. Increasing surface tension coefficient from  $\sigma = 0.067 \text{ N m}^{-1}$  to  $0.0709 \text{ N m}^{-1}$  increases average droplet diameter from  $\bar{d}_d = 0.350 \text{ mm}$  to  $0.397 \text{ mm}$ . The effect of bed size ( $D_b$  and  $\bar{D}_p$ ) has not been studied on the average droplet diameter to the best of the authors knowledge.

Here we study the effect of bed size on the average droplet diameter by conserving the scale-up parameters ( $D_b \omega^2$  and  $Q_i/V_b$ ) constant (according to scale-up criteria

proposed by Liu et al.<sup>[13, 17]</sup>). Figure 9 shows the effect of bed size on the average droplet diameter. At constant values of scale-up criteria ( $D_b \omega^2$  and  $Q_i/V_b$ ), the bed size does not have a significant effect on the average droplet diameter in rotating packed beds. We can also infer that the group of parameters ( $D_b \omega^2$  and  $Q_i/V_b$ ), can be used as scale-up criteria in rotating packed beds to ensure that the the average droplet diameter remains constant.

Nevertheless, it should be mentioned that comparison of the scale-up criterion  $D_b \omega^2$  (proposed by Liu et al.<sup>[13, 17]</sup>), with the dimensionless number  $\Pi_1$  in this work, reveals that  $\bar{D}_p \omega^2$  is a more comprehensive scale-up parameter. In fact, the reason that keeping  $D_b \omega^2$  constant leads to constant average droplet diameters is that the ratio of packing zone length to the bed diameter are constant in our RPB designs. If the ratio of the packing zone length to the bed diameter varies with bed diameter, the scale-up criterion  $\bar{D}_p \omega^2$  should be used instead, since the centrifugal force is applied via the rotation of the packing elements. In other words, changing the bed diameter does not have any effects on the average droplet diameter if the length of the packing zone is kept constant.

## 4 | CONCLUSIONS

This research proposes a correlation for estimation of the average droplet diameter for rotating packed beds. A dataset of experimental and simulation values were used for obtaining the correlation. Effects of rotating speed, absorbent flow rate (i.e. inlet velocity), bed diameter, wire mesh packing diameter, absorbent's viscosity, density and surface tension were considered in this dataset. We used the volume of fluid method to simulate the rotating packed beds and a post-processing code to calculate the average droplet diameter. The results show that the most significant parameters on the average droplet diameter are the rotating speed, centrifugal force and the surface tension, with correlation coefficient of  $R^2 = 0.88$ ,  $0.83$  and  $0.42$ , respectively. This means that the rotating speed, centrifugal force and surface tension mainly govern the average droplet diameter inside rotating packed beds. We performed a dimensional analysis on the studied parameters and observed that the ratio of centrifugal force to the cohesion force is the key dimensionless group in rotating packed beds. The average absolute error of the correlation was equal to 0.138. We also studied the effect of bed size on the average droplet diameter by conserving two scale-up criteria,  $D_b \omega^2$  and  $Q_i/V_b$ , constant. We observed that the bed size does not have a significant effect on the average droplet diameter at constant

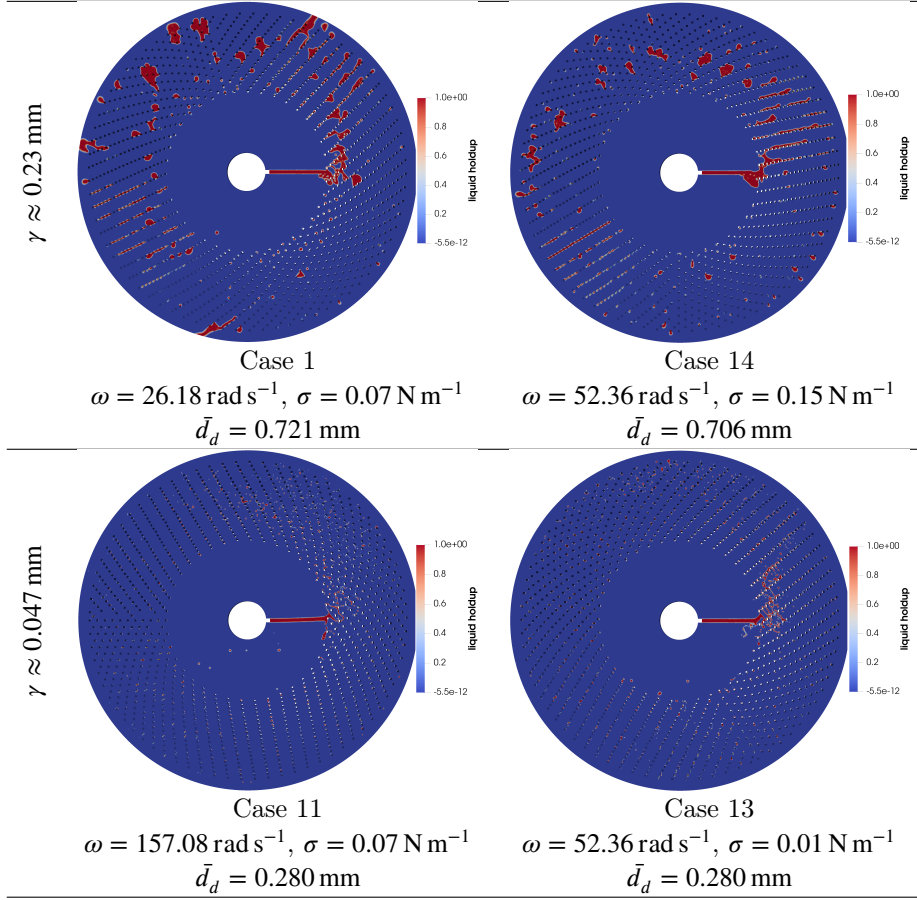


FIGURE 7 Sample screenshots of the RPB simulations operating at similar  $\gamma$  values with different operating conditions (rotation speed and surface tension). Since the  $\gamma$  values are close in cases 1, 14 and 11, 13, the average droplet diameters of these cases are also similar. In cases 1 and 14,  $\gamma \approx 0.23$  mm (which means these RPBs are operating in zone II), while in cases 11 and 13,  $\gamma \approx 0.047$  mm and RPBs are operating in zone I.

values of  $D_b \omega^2$  and  $Q_l/V_b$ . In other words, the group of parameters ( $D_b \omega^2$  and  $Q_l/V_b$ ), can be used as scale-up criteria in rotating packed beds to ensure that the average droplet diameter remains constant. If the ratio of the packing zone length to bed diameter is not kept constant during scale-up, we suggest using  $\bar{D}_p \omega^2$  as the main scale-up criterion instead of  $D_b \omega^2$ . Effect of packing configurations, including the lateral and radial distance of packing elements could be studied as a future work.

## 5 | ACKNOWLEDGEMENTS

The authors would like to acknowledge financial support from the Total and Natural Science and Engineering Research Council (NSERC) through the RGPIN-2020-04510 Discovery Grant. Computations were made on supercomputer Cedar and Graham managed by Compute Canada. In particular, the authors would like to acknowledge the efficient support received from Calcul Québec and Compute Canada systems analysts.

## Nomenclature

$A_d$	Droplet area
$D_b$	Bed diameter

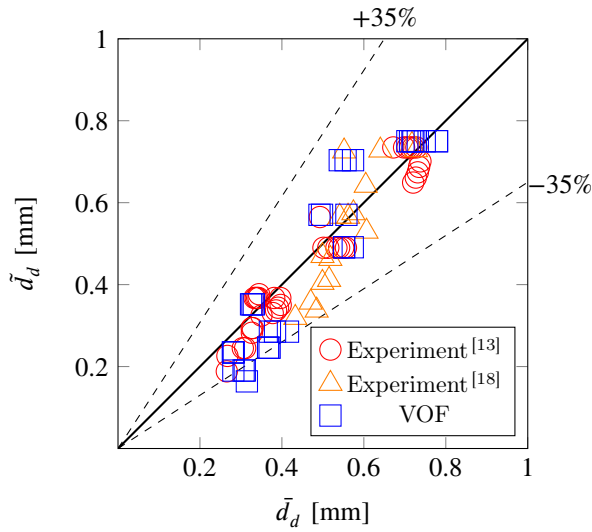


FIGURE 8 Parity plot of the proposed correlation for average droplet diameter.

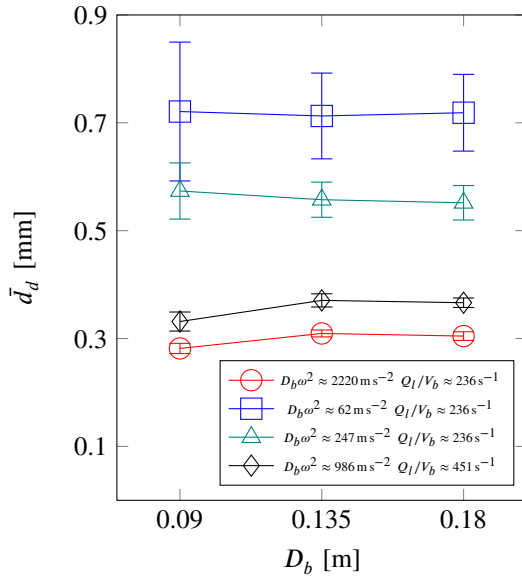


FIGURE 9 Effect of bed diameter ( $D_b$ ) on the average droplet diameter ( $\bar{d}_d$ ) at constant values of  $D_b\omega^2$  and  $Q_l/V_b$ .

$Q_l$	Volumetric flow rate of the absorbent
$R^2$	Coefficient of determination
$R_b$	Bed radius
$S$	Standard deviation
$V_b$	Bed volume

$\bar{D}_p$	Average diameter of the packing zone
$F_C$	Centrifugal force
$F_\sigma$	Surface tension force
$f_\sigma$	Continuum surface force
$g$	Gravitational acceleration
$n_p$	Number of wire mesh packing layers
$u$	Fluid velocity
$\bar{d}_d$	Average droplet diameter
$\tilde{d}_d$	Estimated droplet diameter
$d_p$	Packing diameter
$l_m$	Maximum mesh size
$p$	Pressure
$t$	Time
$x, y$	Sample variables
Greek letters	
$\alpha_i$	Volume fraction of phase $i$
$\bar{\delta}$	Average distance between the wires in a packing
$\gamma$	$\sqrt[3]{\frac{\sigma}{\rho\omega^2}}$
$\mu$	Viscosity
$\omega$	Rotating speed
$\bar{\bar{\tau}}$	Deviatoric stress tensor
$\Pi$	Dimensionless number
$\rho$	Density
$\sigma$	Surface tension coefficient

Subscripts and superscripts

$c1$	Correlation 1
$c2$	Correlation 2
$g$	Gas
$i$	Phase $i$
$l$	Liquid



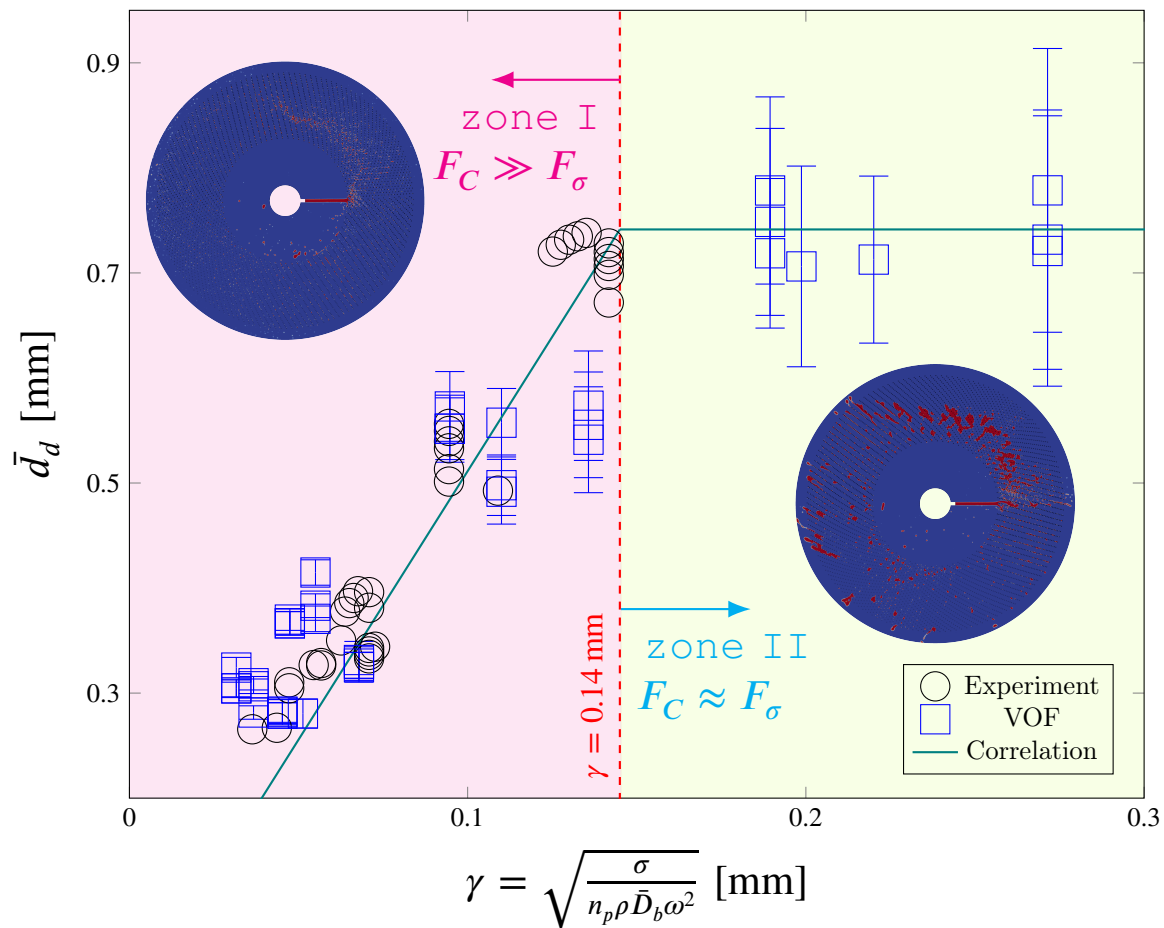



FIGURE 10 Graphical abstract.

## References

- [1] J. Tollefson, Nature 2018, 562, 172.
- [2] P. C. Change, World Meteorological Organization, Geneva, Switzerland 2018, 10.
- [3] A. Yamasaki, Journal of chemical engineering of Japan 2003, 36, 361.
- [4] S. Mirzaei, A. Shamiri, M. K. Aroua, Reviews in Chemical Engineering 2015, 31, 521.
- [5] Z. Qian, Q. Chen, I. E. Grossmann, in Computer Aided Chemical Engineering, volume 44, pp. 2377–2382, Elsevier 2018.
- [6] K. Neumann, K. Gladyszewski, K. Groß, H. Qamar, D. Wenzel, A. Górak, M. Skiborowski, Chemical Engineering Research and Design 2018, 134, 443.
- [7] C. Ramshaw, Chem. Engr. 1983, 389, 13.
- [8] C. Ramshaw, R. Mallinson, Google Scholar There is no corresponding record for this reference.
- [9] Y. Yang, Y. Xiang, G. Chu, H. Zou, Y. Luo, M. Arowo, J.-F. Chen, Chemical Engineering Science 2015, 138, 244.
- [10] Y. Liu, Y. Luo, G.-W. Chu, F. Larachi, H.-K. Zou, J.-F. Chen, Chemical Engineering Journal 2020, 386, 121134.
- [11] P. Xie, X. Lu, D. Ingham, L. Ma, M. Pourkashanian, Energy Procedia 2017, 142, 3407.
- [12] Z.-N. Wen, W. Wu, Y. Luo, L.-L. Zhang, B.-C. Sun, G.-W. Chu, Industrial & Engineering Chemistry Research 2020, 59, 16043.
- [13] W. Liu, Y. Luo, Y.-Z. Liu, G.-W. Chu, Industrial & Engineering Chemistry Research 2020, 59, 5114.



- [14] D. Reay, C. Ramshaw, A. Harvey, Process Intensification: Engineering for efficiency, sustainability and flexibility, Butterworth-Heinemann 2013.
- [15] S. Golshan, R. Rabiee, A. Shams, R. Hoballah, P. Maheshwari, R. Jafari, J. Chaouki, B. Blais,  Industrial & Engineering Chemistry Research 2021.
- [16] Y. Luo, G.-W. Chu, H.-K. Zou, F. Wang, Y. Xiang, L. Shao, J.-F. Chen, Industrial & engineering chemistry research 2012, 51, 9164.
- [17] W. Liu, Y. Luo, Y.-B. Li, G.-W. Chu, Industrial & Engineering Chemistry Research 2020, 59, 5124.
- [18] L. Sang, Y. Luo, G.-W. Chu, J.-P. Zhang, Y. Xiang, J.-F. Chen, Chemical Engineering Science 2017, 158, 429.
- [19] L. Sang, Y. Luo, G.-W. Chu, B.-C. Sun, L.-L. Zhang, J.-F. Chen, AIChE Journal 2019, 65, e16595.
- [20] M.-J. Su, Y. Le, G.-W. Chu, Y.-B. Li, L.-L. Zhang, Y. Luo, Industrial & Engineering Chemistry Research 2020, 59, 3584.
- [21] F. Ghadyanlou, A. Azari, A. Vatani, Sustainability 2021, 13, 8046.
- [22] W. Zhang, P. Xie, Y. Li, L. Teng, J. Zhu, Chemical Engineering and Processing-Process Intensification 2020, 158, 108107.
- [23] Y.-C. Yang, Y. Ouyang, N. Zhang, Q.-J. Yu, M. Arowo, Journal of Chemical Technology & Biotechnology 2019, 94, 1017.
- [24] H. Jasak, A. Jemcov, Z. Tukovic, et al., International workshop on coupled methods in numerical dynamics, volume 1000, IUC Dubrovnik Croatia 2007, pp. 1–20.
- [25] P. Xie, X. Lu, X. Yang, D. Ingham, L. Ma, M. Pourkashanian, Chemical Engineering Science 2017, 172, 216.
- [26] Y. Ouyang, K.-L. Tang, Y. Xiang, H.-K. Zou, G.-W. Chu, R. K. Agarwal, J.-F. Chen, Computers & Fluids 2019, 194, 104296.
- [27] C. W. Hirt, B. D. Nichols, Journal of computational physics 1981, 39, 201.
- [28] J. R. Rygg, CFD analysis of a Pelton turbine in openFOAM, Master's thesis, Institutt for energi-og prosessteknikk 2013.
- [29] X. Liu, Y. Ji, Y. Deng, Y. Wu, Physics of Fluids 2019, 31, 032003.